
Routing on the Stiefel Manifold: When Does Adaptive Subspace Selection Help for Cross-Domain EEG Decoding?

Isabella Costa Maia¹Pedro L. C. Rodrigues²Salem Said³Marco Congedo¹¹GIPSA-lab, University Grenoble Alpes, CNRS, Grenoble-INP²Univ. Grenoble Alpes, Inria, CNRS, Grenoble INP, LJK³Univ. Grenoble Alpes, CNRS, Grenoble INP, LJK

isabella.costa-maia@grenoble-inp.fr pedro.rodrigues@univ-grenoble-alpes.fr
 salem.said@univ-grenoble-alpes.fr marco.congedo@gipsa-lab.grenoble-inp.fr

Abstract

Cross-domain EEG decoding remains challenging despite advances in Riemannian deep learning: covariance matrices from different subjects occupy systematically distinct regions of the SPD manifold, yet existing domain adaptation methods either require target-domain calibration data or learn subject-specific components that cannot generalise across domains. We propose to address this through dynamic Stiefel routing: a pool of K expert projection filters on the Stiefel manifold, each specialised for a different region of the SPD manifold, with each input covariance routed to the most appropriate filter via cross-attention — adapting the subspace projection per sample. A central finding of this work is that this approach, implemented naively, provably collapses to ensemble averaging: when routing weights are uniform, the adaptive filter reduces exactly to an equal-contribution combination of experts, indistinguishable from a single fixed filter. We identify the conditions under which this degeneracy can be broken. Three structural properties are necessary and sufficient: a *symmetric anchor* $W_{\text{base}} \in \text{St}(n, k)$ that removes proximity bias among experts; a *frozen domain-discriminative query encoder* — realised as a domain-separation projection of the log-covariance tangent space — that decouples routing from task optimisation; and a *decoupled key alignment loss* that trains expert keys toward stable domain attractors. Together they produce, to the best of our knowledge, the first genuinely committed and domain-structured routing on SPD manifolds, with consistent gains across three datasets spanning contrasting ratios of dimensionality versus number of domains: balanced accuracy improves from 0.773→0.823, 0.757→0.809, and 0.801→0.839, with the domain-separation projection and alignment strategy determined automatically by a single data-driven rule and no dataset-specific hyperparameter search. A full-rank rectangular extension is indicated, and a concrete implementation path is described.

1 Introduction

The problem. The introduction of Riemannian geometry to brain-computer interfaces marked a turning point in EEG-based motor imagery decoding. By representing neural signals as covariance matrices on the symmetric positive definite manifold $\text{SPD}(n)$ and exploiting its rich metric structure,

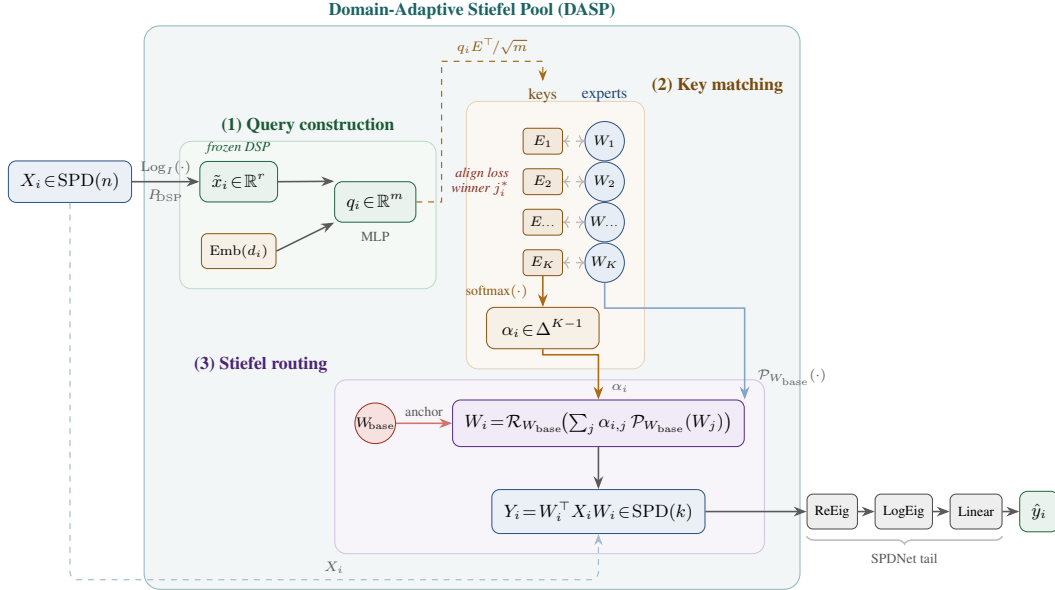


Figure 1: **Domain-Adaptive Stiefel Pool (DASP)** layer overview. (1) *Query construction*: the input covariance X_i is mapped to the tangent space at the identity and projected through a frozen between-domain encoder; the result is concatenated with a learnable domain embedding and passed through an MLP to produce a query q_i . (2) *Key matching*: q_i is compared to a pool of K learnable keys via scaled dot-product, producing routing weights $\alpha_i \in \Delta^{K-1}$; the highest-weighted key is pulled toward q_i by an alignment loss. (3) *Stiefel routing*: a sample-specific filter W_i is obtained by weighted Riemannian interpolation among K expert filters anchored at W_{base} , and applied as a BiMap projection $Y_i = W_i^\top X_i W_i$.

Riemannian methods consistently outperformed conventional feature engineering and established a new state of the art [Barachant et al., 2012, Congedo et al., 2017]. Deep networks soon followed: SPDNet [Huang & Van Gool, 2017] and its successors extended the Riemannian paradigm to learned representations, stacking BiMap, ReEig, and LogEig layers that respect the manifold geometry throughout the forward pass and brought further performance gains.

Despite this progress, cross-domain decoding remains stubbornly plateaued. The main culprit identified with high inter-subject variability: electrode placement, scalp conductivity, neural synchrony patterns, and oscillatory frequency profiles all differ between subjects, causing their covariance matrices to occupy systematically distinct regions of $\text{SPD}(n)$. A model trained on many subjects must simultaneously serve these wildly different input distributions at test time — but the standard BiMap filter $Y = W^\top X W$ with $W \in \text{St}(n, k)$ projects each covariance matrix $X \in \text{SPD}(n)$ through the same fixed subspace, no matter its domain of origin. This is a fundamental design mismatch: the network is geometrically aware of the manifold structure within a subject, yet completely blind to the between-subject structure across the manifold. No matter how deep the architecture becomes, a single shared projection cannot account for the subject-specific region of $\text{SPD}(n)$ each input occupies — and performance saturates as a result. We address this by learning to dynamically route each input covariance to a sample-specific projection at inference time, without retraining or calibration.

An idea and its failure. An idea to address this is to learn K expert filters $\{W_j\}_{j=1}^K \subset \text{St}(n, k)$ and route each input sample to the most appropriate expert via a weighted Riemannian barycenter. We implemented this routing on the Stiefel manifold and immediately encountered a striking failure mode: the routing weights collapse to near-uniform ($\alpha_i \approx 1/K$), and the method reduces to ensemble averaging of a diverse expert pool. The performance gain over the fixed-filter baseline is real — but it comes entirely from having K diverse filters whose mean is better than any single one, not from any per-sample adaptation. This failure is not an accident of initialisation or optimisation. We argue it is a consequence of a fundamental gradient degeneracy: the cross-entropy signal reaching the routing weights α is proportional to the deviation of each expert’s tangent vector from the current weighted mean, which is vanishingly small when experts are similar — and experts remain similar

precisely because they receive no differentiated gradient signal to specialise. Routing collapse and expert homogeneity are self-reinforcing.

Diagnosing and breaking the degeneracy. We introduce a key diagnostic that separates these two regimes: the $K=1$ proxy gap $\Delta_{K=1}$, defined as the difference in balanced accuracy between the adaptive model and the single-expert ensemble baseline evaluated on the same test set. When routing is uniform, $\Delta_{K=1} = 0$ exactly. Positive $\Delta_{K=1}$ is therefore a necessary condition for genuine routing — it cannot be mimicked by ensemble quality alone.

Armed with this diagnostic, we identify three structural properties that taken together break the degeneracy, each motivated by an analogy with Learning to Prompt (L2P) [Wang et al., 2022a] for continual learning:

- (i) A **symmetric anchor** W_{base} that decouples the reference point from the expert pool, removing the W_1 -proximity bias that artificially dampens routing gradients toward one expert.
- (ii) A **frozen domain-discriminative query encoder** — a between-domain separation projection (DSP) of the log-covariance tangent space — that provides routing with domain-identity information independently of the task loss, analogous to L2P’s frozen Visual Transformer (ViT) [Dosovitskiy, et al., 2020] backbone.
- (iii) A **decoupled key alignment loss** that trains expert keys exclusively toward stable query attractors, preventing the moving-target problem that arises when keys compete with classification gradients.

Each component is independently motivated, ablated in isolation, and together they produce, to the best of our knowledge, the first domain-structured routing on SPD manifolds.

Contributions.

- We prove that naive adaptive routing on $\text{St}(n, k)$ collapses to a degenerate solution (uniform weights, single-expert ensemble filter) and characterise the responsible gradient mechanism.
- We propose **Domain-Adaptive Stiefel Pool (DASP)** layer, a drop-in replacement for the standard BiMap layer that combines the three structural fixes above, and introduce the $K=1$ proxy gap as a principled diagnostic for genuine routing value.
- We derive a **unified scaling methodology** for the DSP and alignment loss, governed by the tangent-to-domain ratio ρ , that requires no dataset-specific tuning and generalises across three datasets with $\rho \in \{3.3, 28, 203\}$. Expert count K follows a sub-linear scaling with D that is characterised empirically across our datasets.
- We extend the expert parametrisation to full-rank rectangular matrices and describe two concrete implementation paths.

2 Routing Collapse: The Degenerate Solution

Setup. Let $\mathcal{D} = \{(X_i, y_i, d_i)\}_{i=1}^N$ where $X_i \in \text{SPD}(n)$ is a pre-conditioned EEG covariance matrix, $y_i \in \{1, \dots, C\}$ is the class label, and $d_i \in \{1, \dots, D\}$ is the domain index. Our Domain-Adaptive Stiefel Pool layer maintains K expert filters $\{W_j\}_{j=1}^K \subset \text{St}(n, k)$ and computes attention weights

$$\alpha_i = \text{softmax}(q_i E^\top / \sqrt{m}) \in \Delta^{K-1} \quad (1)$$

where $E \in \mathbb{R}^{K \times m}$ is a learnable matrix of K expert keys, one per expert filter, trained to align with the query vectors of their respective domains, and $q_i \in \mathbb{R}^m$ is a query vector dependent on the input X_i and domain d_i . The j -th component $\alpha_{i,j}$ of α_i gives the weight assigned to expert j for sample i . The layer then applies the per-sample filter via a Riemannian interpolation on the tangent space $\mathcal{T}_{W_{\text{base}}} \text{St}(n, k)$

$$W_i = \mathcal{R}_{W_{\text{base}}} \left(\sum_j \alpha_{i,j} \mathcal{P}_{W_{\text{base}}}(W_j) \right) \quad (2)$$

where $\mathcal{R}_{W_{\text{base}}}(\Delta)$ is the QR retraction of $\Delta \in \mathcal{T}_{W_{\text{base}}} \text{St}(n, k)$ back onto the Stiefel manifold, and $\mathcal{P}_{W_{\text{base}}}(W)$ is the orthogonal projection of $W \in \text{St}(n, k)$ onto the tangent space, both at the basepoint $W_{\text{base}} \in \text{St}(n, k)$.

The degenerate solution. When $\alpha_i = 1/K$ for all samples i , the per-sample filter reduces to:

$$W_i = \mathcal{R}_{W_{\text{base}}} \left(\frac{1}{K} \sum_j \mathcal{P}_{W_{\text{base}}}(W_j) \right) \quad (3)$$

i.e. every sample is projected through the same fixed filter — the one-step approximation of the Fréchet mean of the expert pool. This is exactly the $K=1$ proxy: a single fixed filter that carries no sample-specific information.

If $\alpha_i = 1/K$ for all i , then $W_i = \mathcal{R}_{W_{\text{base}}}(\bar{\Delta})$ is constant across samples, with $\bar{\Delta} = \frac{1}{K} \sum_j \mathcal{P}_{W_{\text{base}}}(W_j)$, and consequently $\text{bAcc}_{\text{adaptive}} = \text{bAcc}_{K=1}$, giving $\Delta_{K=1} = 0$.

Since the $K=1$ proxy uses the same single-expert ensemble filter, the two models produce identical predictions on every input. The $K=1$ proxy gap is therefore a necessary condition for genuine routing: $\Delta_{K=1} = 0$ implies $\alpha_i \approx 1/K$ regardless of absolute accuracy.

Collapse is self-reinforcing. The routing weights α_i are updated by gradients that flow back from the loss through the BiMap output $Y_i = W_i^\top X_i W_i$. Differentiating Y_i with respect to the barycenter weights reveals that the sensitivity of the loss to changing $\alpha_{i,j}$ is proportional to how much expert j deviates from the current mixture in tangent space — that is, how different $\mathcal{P}_{W_{\text{base}}}(W_j)$ is from the interpolated expert $\bar{\Delta}_i = \sum_j \alpha_{i,j} \mathcal{P}_{W_{\text{base}}}(W_j)$. When all experts are similar, every expert’s tangent vector is close to the mean, these deviations are small, and the routing weights receive negligible gradient regardless of how informative the upstream signal is. Crucially, experts remain similar precisely because near-uniform routing gives them identical gradient signals and no pressure to specialise — which in turn keeps their tangent vectors close together, keeping routing gradients weak. Routing collapse and expert homogeneity are mutually reinforcing: neither can resolve without the other moving first.

Empirical evidence. Table 2 (row “Adaptive (naive)”) shows this collapse in practice: on Weibo2014 database [Weibo et al., 2014], $\Delta_{K=1} = -0.00$ despite a +4.5% gain over the fixed-filter baseline. The gain is real but comes entirely from ensemble diversity — the equal-weight barycenter of K diverse experts is a better filter than any single one. The routing mechanism contributes nothing.

3 Domain-Adaptive Stiefel Pool (DASP)

We now describe the three structural fixes that break the degeneracy identified in §2. Each fix has an independent motivation and is validated in isolation in §4.3.

3.1 Fix 1: Symmetric Anchor W_{base}

We introduce a dedicated learnable parameter $W_{\text{base}} \in \text{St}(n, k)$, initialised independently of the expert pool and updated freely by the optimiser while remaining on $\text{St}(n, k)$ via an orthogonal parametrisation. This symmetrises expert competition: no expert has a geometric proximity advantage from the choice of reference point.

3.2 Fix 2: Frozen DSP Query Encoder

A query multi-layer perceptron (MLP) trained end-to-end with cross-entropy learns class-discriminative features — precisely the wrong inductive bias for routing, which requires domain-discriminative features. This is the Riemannian analogue of the core insight behind L2P [Wang et al., 2022a]: its frozen ViT backbone provides task-agnostic, domain-informative queries that decouple key learning from task optimisation.

The between-domain signal in tangent space lives in a subspace of rank at most $D - 1$, where D is the number of training domains. When the tangent space is large relative to D (high $\rho = n(n+1)/(2D)$), this signal is buried in noise and the MLP cannot recover it.

We compute the tangent representation at the identity $I_n \in \text{SPD}(n)$ as $x_i = \text{upper}(\log(X_i)) \in \mathbb{R}^{n(n+1)/2}$, where $\log(\cdot)$ denotes the matrix logarithm and $\text{upper}(\cdot)$ extracts the upper-triangular part

with $\sqrt{2}$ -scaled off-diagonal entries [Penneç et al., 2006]. Then, we project x_i through a frozen matrix:

$$P_{\text{DSP}} \in \mathbb{R}^{n(n+1)/2 \times r}, \quad \text{columns} = \text{top-}r \text{ DSP filter eigenvectors of } S_B \quad (4)$$

where $S_B = \sum_{d=1}^D n_d (\mu_d - \mu)(\mu_d - \mu)^\top$ is the between-domain scatter matrix, computed once from training tangent-space representations and frozen. P_{DSP} carries no gradient; it acts as a fixed domain-discriminative feature extractor analogous to L2P’s frozen ViT. We use $r = 40$ to span both the $D-1$ between-domain directions and additional within-domain structure (§4.3). We denote the (optionally projected) tangent vector as

$$\tilde{x}_i = \begin{cases} x_i P_{\text{DSP}} & \text{if } \rho > \rho^* \\ x_i & \text{if } \rho \leq \rho^* \end{cases} \quad (5)$$

so that $\tilde{x}_i \in \mathbb{R}^r$ in the high- ρ regime and $\tilde{x}_i \in \mathbb{R}^{n(n+1)/2}$ in the low- ρ regime.

3.3 Fix 3: Decoupled Key Alignment Loss

Even with a stable, domain-informative query, expert keys trained via cross-entropy receive a moving target: the task loss pushes keys toward whatever representation helps classification, which may not align with domain identity. We instead train keys exclusively via a surrogate alignment loss:

$$\mathcal{L}_{\text{align}} = \lambda_{\text{align}} \mathbb{E}_i \left[1 - \cos(\text{sg}(q_i), E_{j_i^*}) \right], \quad j_i^* = \arg \max_j \alpha_{i,j} \quad (6)$$

where $\text{sg}(\cdot)$ denotes stop-gradient on the query (analogous to L2P’s frozen query function), and only the highest-weighted key $E_{j_i^*}$ is updated per sample. Pulling all keys toward every query simultaneously would cause key collapse toward the global mean, defeating the purpose of the pool; the winner-take-all update instead creates competitive pressure for keys to specialise toward their respective domains. When `decouple_keys=True`, E is additionally detached from the cross-entropy gradient path entirely, so keys are optimised *exclusively* by $\mathcal{L}_{\text{align}}$ toward stable per-domain attractors. The total loss is $\mathcal{L} = \mathcal{L}_{\text{CE}} + \mathcal{L}_{\text{align}}$.

3.4 The Full Layer

The complete **DASP** layer is shown in Figure 1. It takes as input a batch of SPD matrices $\{X_i\} \subset \text{SPD}(n)$ and domain indices $\{d_i\}$, and returns $Y_i = W_i^\top X_i W_i \in \text{SPD}(k)$, where the per-sample filter W_i is the attention-weighted Riemannian interpolation of Eq. (2), with weights α_i from Eq. (1). The three components below specify how q_i , W_{base} , and the manifold operations are instantiated.

Query construction. The query q_i (Eq. 1) is formed by combining the projected tangent vector \tilde{x}_i (Eq. 5) with a learnable domain embedding

$$q_i = \text{MLP}([\tilde{x}_i; \text{Emb}(d_i)]) \in \mathbb{R}^m \quad (7)$$

where the MLP has one hidden layer of dimension $2m$ with GELU activation.

Dedicated anchor. The reference point W_{base} in Eqs. 2–3 is instantiated as the dedicated learnable parameter $W_{\text{base}} \in \text{St}(n, k)$ described in §3.1, replacing the dynamic one-step barycenter of naive routing.

Manifold operations. Since the true Riemannian log-map on $\text{St}(n, k)$ has no closed form, we use the tangent projection as a first-order approximation

$$\mathcal{P}_{W_{\text{base}}}(W) = W - W_{\text{base}} \text{sym}(W_{\text{base}}^\top W) \in \mathcal{T}_{W_{\text{base}}} \text{St}(n, k) \quad (8)$$

where $\text{sym}(A) = \frac{1}{2}(A + A^\top)$ denotes the symmetric part of A .

The QR retraction maps tangent vectors back onto the manifold: letting $W_{\text{base}} + \Delta = QR$ be the thin QR decomposition

$$\mathcal{R}_{W_{\text{base}}}(\Delta) = Q \in \text{St}(n, k) \quad (9)$$

Both are valid approximations of the true log and exp maps when W_{base} and the target are not too far apart [Edelman et al., 1998, Absil et al., 2008]. The BiMap output $Y_i = W_i^\top X_i W_i \in \text{SPD}(k)$ is then fed to the standard $\text{ReEig} \rightarrow \text{LogEig} \rightarrow \text{Linear tail}$ [Huang & Van Gool, 2017].

Table 1: Unified scaling methodology. $\rho = n(n+1)/(2D)$ is the tangent-to-domain ratio. The DSP and alignment strategy are determined automatically by ρ with no dataset-specific tuning; expert count K follows an empirical sub-linear scaling with D .

Parameter	Rule	Condition
K	sub-linear in D ; see section A	always
d_{emb}	20	always
DSP	enabled, $r = 40$	$\rho > 50$
DSP	disabled	$\rho \leq 50$
λ_{align}	0.05, <code>decouple_keys=True</code>	$\rho > 50$

3.5 Routing Diagnostics

Three diagnostics track whether routing is genuine or degenerate:

K=1 proxy gap $\Delta_{K=1} = \text{bAcc}_{\text{adaptive}} - \text{bAcc}_{K=1}$, where $\text{bAcc}_{K=1}$ is the accuracy of W_{base}^\dagger (the single equal-contribution filter) evaluated on the *test* set. $\Delta_{K=1} = 0$ iff routing is uniform; positive values in a majority of cross-validation folds constitute our success criterion.

Routing entropy $\bar{H} = \mathbb{E}_i \left[\frac{H(\alpha_i)}{\log K} \right] \in [0, 1]$: near 1 is uniform (degenerate); near 0 is one-hot (committed).

Domain alignment ratio $r_d = \text{Var}_d(\bar{\alpha}_d) / \text{Var}_i(\alpha_i)$, where $\bar{\alpha}_d = \frac{1}{|I_d|} \sum_{i: d_i=d} \alpha_i \in \Delta^{K-1}$ is the mean routing vector for domain d : values above 0.10 indicate domain-structured routing.

3.6 Unified Scaling Methodology

The degree to which domain identity is recoverable from the tangent space depends on the *tangent-to-domain ratio*

$$\rho = \frac{n(n+1)/2}{D} \quad (10)$$

When $\rho \gg 1$, domain identity is buried in high-dimensional noise and the DSP is essential. When $\rho \approx 1$, the tangent space is compact relative to the number of domains, and the query MLP finds domain structure unaided. A threshold $\rho^* = 50$ cleanly separates these regimes across all three datasets, determining whether the DSP projection and alignment loss are activated. In the high- ρ regime, expert keys must be decoupled from the cross-entropy gradient (`decouple_keys=True`) so that the alignment loss can train them exclusively toward stable domain attractors, as described in §3.3. In the low- ρ regime, the alignment loss is disabled and `decouple_keys=False` ensures that keys still receive a training signal from the classification objective. Expert count K follows a sub-linear scaling with D : empirically, $K \approx D - 1$ works well for small D ($D \leq 10$) and $K \approx D/2$ for larger D ($D \geq 20$), reflecting diminishing returns in routing capacity as the number of domains grows. Exact values per dataset are given in section A. These rules are summarised in Table 1.

4 Experiments

4.1 Setup

We evaluate on three motor imagery datasets with contrasting geometry, spanning the low- and high- ρ regimes. All experiments use the Adam optimiser [Kingma & Ba, 2015] at learning rate 0.01, batch size 32, and 5-fold cross-validation with 70/15/15% trial-level train/val/test splits. The primary metric is balanced accuracy (bAcc). We consider binary classification between *right-hand* and *feet* motor imagery across all datasets. Raw EEG signals are bandpass filtered between 8 and 32 Hz and subjected to an adaptive amplitude thresholding artifact rejection. Covariance matrices are then pre-conditioned per domain by a sequence of three operations: Tikhonov regularization (diagonal loading) with parameter 10^{-8} , whitening using the Euclidean mean of the training set and multiplied by the ratio $\text{trace}/\text{squared Frobenius norm}$.

Table 2: Main results. **Key diagnostic:** $\Delta_{K=1} > 0$ measures genuine routing value. The naive model gains from ensemble diversity but not routing ($\Delta_{K=1} \approx 0$ on Weibo2014). Our method achieves consistent positive $\Delta_{K=1}$ across all three datasets. †: unified methodology applied. Folds: indicate the ratio of cross-validation folds with $\Delta_{K=1} > 0.01$.

Dataset	Model	bAcc	Std	Δ_{base}	$\Delta_{K=1}$	Folds	\bar{H}	r_d
Weibo2014	Baseline BiMap	0.773	0.020	—	—	—	—	—
	Adaptive (naive)	0.818	0.031	+0.045	−0.00	0/5	0.836	0.281
	DASP (Ours)†	0.823	0.011	+0.050	+0.029	4/5	0.674	0.710
BNCI2015001	Baseline BiMap	0.757	0.017	—	—	—	—	—
	Adaptive (naive)	0.796	0.012	+0.040	+0.050	5/5	0.494	0.888
	DASP (Ours)†	0.809	0.009	+0.053	+0.247	5/5	0.482	0.539
BNCI2014001	Baseline BiMap	0.801	0.023	—	—	—	—	—
	DASP (Ours)†	0.839	0.009	+0.038	+0.170	5/5	0.597	0.828

Stiefel-constrained parameters are maintained via the orthogonal parametrisation of [Paszke et al., 2019]. SPDNet layers (BiMap, ReEig, LogEig), and operations like the matrix logarithm are provided by the `spd_learn` library [Aristimunha et al., 2026]. The baseline is a standard single-stage SPDNet [Huang & Van Gool, 2017] with a fixed BiMap layer applying the same subspace dimension k as our method.

All experiments were run on a single CPU workstation (Intel Core i7, 32 GB RAM). Each 5-fold cross-validation run takes approximately 20–30 minutes for Weibo2014 ($n=60$) and 5–10 minutes for the BNCI datasets ($n \leq 22$). The full ablation study (Table 3, 6 configurations \times 5 folds) required approximately 3 hours of compute. No GPU was used.

Weibo2014 [Weibo et al., 2014]: $n=60$, $D=9$, $K=8$, $\rho=203$. High- ρ regime; DSP essential.

BNCI2015001 [Faller et al., 2012]: $n=13$, $D=28$, $K=16$, $\rho=3.3$. Low- ρ regime; domain structure naturally accessible.

BNCI2014001 [Tangermann et al., 2012]: $n=22$, $D=9$, $K=8$, $\rho=28$. Low- ρ regime; sits near the $\rho^*=50$ boundary, testing the scaling rule at an intermediate channel count.

Subspace dimension k . The output dimension k of the BiMap layer controls the degree of dimensionality reduction applied to the covariance matrices. For Weibo2014 ($n=60$) we use $k=30$, halving the input dimension following standard practice in SPDNet-based decoding [Huang & Van Gool, 2017]. For the BNCI datasets ($n=13$, $n=22$) the input dimension is already compact, and aggressive reduction would discard between-domain discriminative structure needed by the routing mechanism. We therefore use more conservative reductions: $k=12$ for BNCI2015001 and $k=20$ for BNCI2014001, preserving a larger fraction of the tangent space geometry. Exact values are reported in section A.

4.2 Main Results

Table 2 tells a clear story. The naive adaptive model improves over the fixed-filter baseline on all datasets, but on Weibo2014 the $K=1$ proxy gap is zero: every percentage point of gain comes from ensemble diversity, none from routing. Our full method breaks this degeneracy: $\Delta_{K=1}$ is positive in 4 out of 5 folds on Weibo2014 (+0.029) and in 5 out of 5 folds on both BNCI datasets (+0.247, +0.170). Routing entropy confirms the transition from degenerate ($\bar{H} = 0.836$) to committed ($\bar{H} = 0.674$) routing on Weibo2014, while domain alignment ($r_d = 0.710$) confirms the routing is structured by subject identity, not noise.

A secondary pattern is notable: $\Delta_{K=1}$ is substantially larger in the low- ρ regime (+0.247, +0.170) than in the high- ρ regime (+0.029). In the low- ρ regime the compact tangent space enables expert specialisation, making the single-expert ensemble filter a poor proxy and per-sample routing highly valuable.

LOSO generalisation results and directions for future work are presented in Appendices C and D.

Table 3: Ablation on Weibo2014 ($K=8, k=30, n=60$). Primary criterion: $\Delta_{K=1} > 0.01$ in at least 3 out of 5 folds (\dagger). Load-balancing (B1) is a negative control: it *maximises* entropy, confirming that sharpness alone is not sufficient. Each component independently contributes; the full method achieves all three diagnostic targets simultaneously.

ID	Configuration	bAcc	Δ_{base}	$\Delta_{K=1}$	\bar{H}	r_d
Ref	Naive adaptive	0.818	+0.045	−0.000	0.836	0.281
— Each fix in isolation —						
B1	+ load-balance loss	0.818	+0.045	+0.001	0.973	0.288
B2	+ entropy loss	0.819	+0.046	+0.006	0.768	0.278
B4	+ alignment loss only	0.818	+0.045	−0.000	0.853	0.386
B12 \dagger	+ W_{base} only	0.805	+0.032	+0.027	0.884	0.335
DSP \dagger	+ W_{base} + DSP	0.810	+0.037	+0.016	0.776	0.690
— Full method —						
DASP (Ours)\dagger	W_{base} + DSP + align + decouple	0.823	+0.050	+0.029	0.674	0.710

4.3 Ablation: What Breaks the Degeneracy?

We follow a strict one-factor-at-a-time protocol on Weibo2014. The results expose a clear causal chain (Table 3).

Load-balancing loss (B1) is a negative control. The Switch Transformer load-balancing loss [Fedus et al., 2022] is minimised at uniform routing, pushing entropy toward 0.973. $\Delta_{K=1}$ remains zero. This confirms our claim: high entropy causes degeneracy; we cannot resolve it by pushing entropy further up. The only path forward is to provide routing with information about what to differentiate — which requires structural, not just loss-level, changes.

W_{base} is the most impactful single change. Replacing the W_1 -anchored reference point with a dedicated symmetric anchor immediately produces $\Delta_{K=1} = +0.027$ (3 out of 5 folds), while domain alignment climbs from 0.281 to 0.335. The mechanism is geometric: symmetrising expert competition allows all K experts to receive equal gradient signal, enabling specialisation.

Frozen DSP amplifies the domain signal. Adding the DSP on top of W_{base} causes domain alignment to jump from 0.335 to 0.690, confirming that the projection provides the stable, domain-discriminative query signal needed for key convergence. Without it, the query MLP learns class-discriminative features that happen to be domain-informative only incidentally.

Alignment loss + decoupled keys seals the convergence. Alignment alone (B4, without W_{base}) raises domain alignment but not $\Delta_{K=1}$, because the query provides a moving target. Combined with W_{base} and DSP, alignment produces the full method’s entropy of 0.674 and domain alignment of 0.710 — both conditions for domain-structured committed routing satisfied simultaneously.

4.4 Validation of the Scaling Methodology

BNCI2014001 ($\rho = 28 < \rho^*$) behaves identically to BNCI2015001 ($\rho = 3.3$) despite a $7\times$ higher ratio: routing is domain-structured without DSP ($r_d = 0.828$), and adding DSP hurts rather than helps, confirming that the scaling rule generalises to intermediate channel counts. The contrast with Weibo2014 ($\rho = 203$) is sharp: without DSP, the query MLP cannot extract domain identity from the 1830-dimensional tangent space and routing collapses ($\Delta_{K=1} \approx 0$).

5 Full-Rank Rectangular Extension

The Stiefel constraint $W_j \in \text{St}(n, k)$ restricts each expert to the orthonormal group, preserving subspace orientation but precluding per-direction amplitude scaling. We describe here a theoretical generalisation to full-rank rectangular experts that we leave for empirical validation to future work (see §D).

The idea is to learn full-rank rectangular experts $W_j \in \mathbb{R}^{n \times k}$, so that the Domain-Adaptive Pool layer $Y = W_j^\top X W_j$ additionally encodes re-colouring transformation of the projected covariance. The space of full-rank rectangular matrices can be identified with the product of the Stiefel manifold $\text{St}(n, k)$ and the cone of symmetric positive definite matrices $\text{SPD}(k)$, making this a strict generalisation of the Stiefel prompt pool.

Implementation path 1 — Pseudo-polar decomposition. Each expert is factored as $W_j = Q_j P_j^{1/2}$, where $Q_j \in \text{St}(n, k)$ is an orthonormal factor maintained on the Stiefel manifold as before, and $P_j \in \text{SPD}(k)$ is a learnable symmetric positive definite matrix. The BiMap becomes $Y = P_j^{1/2} Q_j^\top X Q_j P_j^{1/2}$, separating the rotation (Q_j) from the scaling (P_j) components. P_j can be parametrised via its Cholesky factor to guarantee positive definiteness throughout training [Absil et al., 2008, Golub & Van Loan, 2013].

Implementation path 2 — Barrier regularisation. Alternatively, each expert $W_j \in \mathbb{R}^{n \times k}$ is learned as an unconstrained parameter, with a log-determinant barrier term added to the loss to enforce full column rank:

$$\mathcal{L}_{\text{barrier}} = -\lambda_{\text{barrier}} \sum_{j=1}^K \log \det(W_j^\top W_j) \quad (11)$$

As W_j approaches rank deficiency, $\det(W_j^\top W_j) \rightarrow 0$ and $\mathcal{L}_{\text{barrier}} \rightarrow +\infty$, creating an implicit manifold boundary that keeps experts full-rank without hard parametrisation. This approach requires no manifold-aware optimiser and is readily compatible with the existing training pipeline.

6 Related Work

Riemannian deep learning for EEG. SPDNet [Huang & Van Gool, 2017] and extensions [Brooks et al., 2019, Kobler et al., 2022] operate on SPD manifolds via BiMap, ReEig, and LogEig layers. Domain adaptation approaches include covariance recentering [Zanini et al., 2017], Riemannian batch normalisation [Brooks et al., 2019], and Riemannian Procrustes Analysis [Rodrigues et al., 2019] — all requiring target-domain calibration data. Our method requires no test-time calibration and is, to the best of our knowledge, the first to achieve genuine input-adaptive routing on the SPD manifold.

Mixture of experts. Sparse MoE [Shazeer et al., 2017] and Switch Transformer [Fedus et al., 2022] use learned gating with load-balancing losses that encourage *uniform* utilisation — the opposite of our goal. We show explicitly (Table 3, B1) that applying such losses to our setting drives routing toward the degenerate solution.

Prompt-based continual learning. L2P [Wang et al., 2022a] and DualPrompt [Wang et al., 2022b] select prompts via frozen pre-trained feature queries. Our work translates the key structural principles (frozen query, decoupled key training, alignment loss) from the Euclidean token setting to the Riemannian geometry of SPD manifolds.

7 Conclusion

We studied the problem of per-sample adaptive subspace selection in Riemannian deep learning for EEG decoding. Our central finding is that naive adaptive routing on the Stiefel manifold is provably degenerate: uniform weights reduce the layer to a single equal-experts-contribution filter, indistinguishable from the fixed-filter baseline in terms of per-sample adaptation. The $K=1$ proxy gap — the accuracy difference between the adaptive model and this degenerate solution — is the only diagnostic that separates genuine routing from ensemble averaging.

Three structural properties borrowed from Learning to Prompt break the degeneracy: a symmetric anchor, a frozen domain-discriminative query encoder, and a decoupled key alignment loss. Together they produce the first committed ($\bar{H} = 0.67$) and domain-structured ($r_d = 0.71$) routing on SPD manifolds, with consistent accuracy gains across three datasets of contrasting geometry. A unified

data-driven scaling rule — governed by the tangent-to-domain ratio ρ — eliminates dataset-specific tuning.

References

- Barachant, A., Bonnet, S., Congedo, M., and Jutten, C. Multiclass brain-computer interface classification by Riemannian geometry. *IEEE Trans. Biomed. Eng.*, 59(4):920–928, 2012.
- Blankertz, B., Tomioka, R., Lemm, S., Kawanabe, M., and Müller, K.-R. Optimizing spatial filters for robust EEG single-trial analysis. *IEEE Signal Process. Mag.*, 25(1):41–56, 2008.
- Brooks, D., Schwander, O., Barbaresco, F., Schneider, J.-Y., and Cord, M. Riemannian batch normalization for SPD neural networks. *NeurIPS*, 32, 2019.
- Edelman, A., Arias, T. A., and Smith, S. T. The geometry of algorithms with orthogonality constraints. *SIAM J. Matrix Anal. Appl.*, 20(2):303–353, 1998.
- Fedus, W., Zoph, B., and Shazeer, N. Switch transformers: Scaling to trillion parameter models with simple and efficient sparsity. *JMLR*, 23(1):1–39, 2022.
- Huang, Z. and Van Gool, L. A Riemannian network for SPD matrix learning. *AAAI*, 2017.
- Kobler, R. J., Hirayama, J.-I., Zhao, Q., and Kawanabe, M. SPD domain-specific batch normalization to crack interpretable unsupervised domain adaptation in EEG. *NeurIPS*, 35, 2022.
- Rodrigues P. L. C., et al. Riemannian Procrustes Analysis: Transfer Learning for Brain–Computer Interfaces *IEEE Transactions on Biomedical Engineering*, vol. 66, no. 8, pp. 2390-2401, Aug. 2019.
- Shazeer, N. et al. Outrageously large neural networks: The sparsely-gated mixture-of-experts layer. *ICLR*, 2017.
- J. Faller, C. Vidaurre, T. Solis-Escalante, C. Neuper and R. Scherer, Autocalibration and Recurrent Adaptation: Towards a Plug and Play Online ERD-BCI *IEEE Transactions on Neural Systems and Rehabilitation Engineering*, vol. 20, no. 3, pp. 313-319, May 2012.
- Tangermann, M. et al. Review of the BCI competition IV. *Front. Neurosci.*, 6:55, 2012.
- Wang, Z. et al. Learning to prompt for continual learning. *CVPR*, 2022.
- Wang, Z. et al. DualPrompt: Complementary prompting for rehearsal-free continual learning. *ECCV*, 2022.
- Zanini, P. et al. Transfer learning: A Riemannian geometry framework with applications to BCIs. *IEEE Trans. Biomed. Eng.*, 65(5):1107–1116, 2017.
- Congedo, M. et al. Riemannian geometry for EEG-based brain-computer interfaces; a primer and a review. *Brain-Computer Interfaces*, 4(3), 155–174.
- Dosovitskiy, et al. An image is worth 16x16 words: Transformers for image recognition at scale. *arXiv preprint arXiv:2010.11929*, 2020.
- Yi, Weibo, et al. Evaluation of EEG oscillatory patterns and cognitive process during simple and compound limb motor imagery. *PloS*, one 9.12 (2014): e114853.
- Paszke, A., Gross, S., Massa, F., Lerer, A., Bradbury, J., Chanan, G., Killeen, T., Lin, Z., Gimelshein, N., Antiga, L., et al. PyTorch: An imperative style, high-performance deep learning library. *Advances in Neural Information Processing Systems*, 32, 2019.
- Kingma, D. P. and Ba, J. Adam: A method for stochastic optimization. *International Conference on Learning Representations*, 2015.
- Absil, P.-A., Mahony, R., and Sepulchre, R. Optimization Algorithms on Matrix Manifolds. *Princeton University Press*, 2008.

Golub, G. H. and Van Loan, C. F. Matrix Computations. *Johns Hopkins University Press*, 4th edition, 2013.

Aristimunha, B. et al. SPD Learn: A Geometric Deep Learning Python Library for Neural Decoding Through Trivialization. *arXiv preprint arXiv:2602.22895*, 2026.

Gallet, M., Bouchard, F., Mian, A., and Ginolhac, G. ARMAGNAC: A New Parametric Batch Normalization Layer for SPDNet Architecture. *HAL preprint hal-05529546*, 2026.

Pennec, X., Fillard, P., Ayache, N. A Riemannian framework for tensor computing. *Int J Comput Vision*, 66(1):41–66, 2006.

A Hyperparameter Summary

Table 4: Hyperparameters per dataset. Ablations freeze all except the factor under test.

Param	Weibo2014	BNCI2015001	BNCI2014001	Description
n	60	13	22	Input SPD dimension
k	30	12	20	Output SPD dimension
K	8	16	8	Expert filters
m	20	20	20	Query/key/emb dim
r	40	0	0	DSP dim
λ_{align}	0.05	0.0	0.0	Alignment weight
decouple	True	False	False	Key gradient decoupling
lr	0.01	0.01	0.01	Adam [Kingma & Ba, 2015]
Batch	32	32	32	
Epochs	40	40	40	Max, patience 10

B Diagnostic Metric Definitions

Routing entropy. $\bar{H} = \frac{1}{N \log K} \sum_i H(\alpha_i)$, where $H(\alpha_i) = -\sum_j \alpha_{i,j} \log \alpha_{i,j}$. Threshold $\bar{H} < 0.70$ indicates sharp routing.

Domain alignment ratio. $r_d = \text{Var}_d(\bar{\alpha}_d) / \text{Var}_i(\alpha_i)$, where $\bar{\alpha}_d = \frac{1}{|I_d|} \sum_{i: d_i=d} \alpha_i$ is the mean routing vector for domain d , and $|I_d|$ is the number of samples belonging to domain d . Values above 0.10 indicate domain-structured routing.

Expert diversity. Mean principal angle between column spaces of all expert pairs, computed via SVD of $W_j^\top W_{j'}$ for all $j \neq j'$. Values near 45° indicate maximal diversity; near 0° indicates collapse.

K=1 proxy. The equal-expert contribution W_{base}^\dagger used as a single shared filter, evaluated on the *test* set. $\Delta_{K=1} > 0.01$ in $\geq 3/5$ folds is the success criterion for genuine routing beyond ensemble averaging.

C LOSO Generalisation

Evaluation paradigm. The main paper evaluates under a *cross-domain* protocol using a cross-validation procedure: all D domains (combination of subject-session) are seen during training, and test samples are drawn from the same domain pool. This protocol measures how well the routing mechanism adapts to known domains at test time, and is the standard evaluation in SPDNet-based motor imagery decoding [Huang & Van Gool, 2017].

A strictly harder paradigm is *leave-one-subject-out* (LOSO): each fold holds out one subject entirely from training, and the model must classify trials from a subject it has never seen. This is a genuine

zero-shot transfer setting — the domain embedding $\text{Emb}(d_i)$ is undefined for the held-out subject, and the routing mechanism must operate without subject-specific supervision. LOSO therefore tests a fundamentally different capability: whether the routing generalises beyond the training domain distribution, rather than adapting within it.

Protocol. We evaluate on Weibo2014 ($D = 9$, 8 LOSO folds, one subject held out per fold). Since the domain embedding cannot be used for the unseen subject, we compare four inference strategies:

- **Baseline BiMap:** fixed filter, no routing.
- **Condition A — Input-only:** `use_domain_emb=False`; routing driven solely by the frozen between-domain encoder \tilde{x}_i , with no domain embedding. This is the most principled zero-shot strategy since it uses only information available at test time.
- **Condition B — Zero-mask:** domain embedding zeroed for the held-out subject ($\text{Emb}(d_{\text{new}}) = \mathbf{0}$).
- **Condition C — NN-inference:** domain embedding initialised as the embedding of the nearest training subject, measured by L2 distance between subject-level tangent-space means.

Table 5: LOSO results on Weibo2014 (8 folds). Baseline BiMap: 0.779 ± 0.087 .

Condition	Description	bAcc	Std
Baseline BiMap	Fixed filter	0.779	0.087
Adaptive (full)	Domain emb for train subj.	0.770	0.080
A — Input-only	No domain emb	0.776	0.074
B — Zero-mask	Domain emb zeroed	0.771	0.081
C — NN-inference	Nearest training subject	0.768	0.098

Discussion. No adaptive variant consistently beats the baseline under LOSO, confirming that the method is designed for the cross-domain paradigm where subject identity is known at training time. The gap between the cross-domain result (0.823) and the best LOSO result (0.776) reflects the fundamental difficulty of zero-shot transfer: the routing mechanism learns domain attractors during training, and these attractors do not automatically generalise to unseen subjects.

The best strategy is input-only routing (Condition A, -0.003 vs baseline, within variance), where the frozen between-domain encoder alone provides sufficient structure to make soft routing decisions without any domain supervision. This confirms that the encoder captures some subject-agnostic geometric structure in the tangent space, but not enough to match the performance achievable when the subject is known.

NN-based domain inference (Condition C) does not improve over zero-masking (0.768 vs 0.771), because L2 distance in tangent space is not a reliable proxy for routing similarity. A more geometrically principled alternative — computing the affine-invariant Riemannian distance $d(X, Y) = \|\log(X^{-1/2}YX^{-1/2})\|_F$ between subject-level Fréchet means on $\text{SPD}(n)$ — is a natural direction for future work.

The tangent space projection at the identity I_n used in the query encoder is justified by the per-domain pre-conditioning applied to the covariance matrices (whitening and variance equalisation), which recenters each domain’s distribution around I_n before the network sees the data. Incorporating recentering directly within the model via a Riemannian batch normalisation layer [Brooks et al., 2019, Gallet et al., 2026] is a natural extension that would remove the dependency on external pre-conditioning and remains an open direction.

D Future Work

Top- p sparse routing. Current routing computes a soft barycenter over all K experts for every sample, diluting gradient signals and making expert specialisation harder. Replacing the softmax over all K with a masked softmax over the top- p experts (straight-through estimator for the selection boundary) would create genuine winner-take-all pressure, analogous to L2P’s top- N prompt selection, and is expected to produce sharper routing without requiring additional losses.

Transductive LOSO adaptation. The most promising near-term direction for improving LOSO performance is transductive inference: given a batch of unlabelled test samples from an unseen subject, optimise only the domain embedding $\text{Emb}(d_{\text{new}})$ for a small number of gradient steps on an unsupervised objective (e.g. routing entropy minimisation). All other parameters remain frozen. This requires no architectural changes and directly exploits the routing structure learned during training.

Riemannian NN-inference. Replacing L2 tangent-space distance with the affine-invariant Riemannian distance $d(X, Y) = \|\log(X^{-1/2}YX^{-1/2})\|_F$ between subject-level Fréchet means on $\text{SPD}(n)$ would give nearest-neighbour domain initialisation a more principled geometric basis, potentially improving Condition C in the LOSO setting.

Full-rank rectangular expert routing. Section 5 introduces the full-rank rectangular generalisation of Stiefel expert routing and describes two concrete implementation paths; validating this extension empirically on non-pre-conditioned data, where between-subject amplitude differences are preserved, remains an open direction.

Per-domain Common Spatial Patterns (CSP) targets. Maintaining a running exponential-moving average of per-domain per-class covariance estimates and computing domain-specific CSP targets would give routing supervision a stable per-domain attractor compatible with the alignment loss [Blankertz et al., 2008], addressing the instability observed with batch-level CSP supervision.